ISSN 1990-7931, Russian Journal of Physical Chemistry B, 2007, Vol. 1, No. 6, pp. 588–599. © Pleiades Publishing, Ltd., 2007.
Original Russian Text © A.P. Ershov, N.P. Satonkina, G.M. Ivanov, 2007, published in Khimicheskaya Fizika, 2007, Vol. 26, No. 12, pp. 21–33.

COMBUSTION AND EXPLOSION

# Electroconductivity Profiles in Dense High Explosives

**A. P. Ershov, N. P. Satonkina, and G. M. Ivanov**

*Lavrent'ev Institute of Hydrodynamics, Siberian Branch, Russian Academy of Sciences, pr. Akademika Lavrent'eva 15, Novosibirsk, 630090 Russia*

*e-mail: ers@hydro.nsc.ru*

Received December 7, 2006

**Abstract**—A method for measuring the electroconductivity profiles behind the detonation front in dense solid high explosives with a resolution of 0.1 mm was developed. The method has a measurement range more than an order of magnitude wider than the available methods. During the detonation of pressed PETN, RDX, and HMX, an electroconductivity peak with an amplitude of several $\Omega^{-1}$ cm$^{-1}$ and a width of 40 to 70 ns was observed. The peak width is in agreement with the available data on the width of the chemical reaction zone. The peak is accompanied by a tail with an electroconductivity several times lower.

**DOI:** 10.1134/S1990793107060139

## 1. INTRODUCTION

The kinetics of the chemical reactions driving the detonation of high explosives (HEs) has been of permanent interest for decades. Data on the width and structure of the reaction zone are quite often contradictory, not a surprising situation, since the problem of characterizing the reaction zone is one of the most difficult to tackle in the physics of explosion. A high reaction rate or, equivalently, a narrow reaction zone needs a high spatial resolution to make it accessible to experimental observations. Note also that the harsh conditions behind the detonation wave hamper the use of small-size sensors. On the other hand, the use of optical methods, characterized by a high resolution, the process may be complicated by the interaction of the detonation wave with the material of the observation windows. Therefore, the development of alternative methods is of considerable importance. This work describes a method for measuring the distribution of electric conductivity and some results obtained by its use.

About sixty years ago, the authors of [1] demonstrated that the medium behind the detonation front possesses a high electric conductivity. The results obtained in [2, 3] revealed that the electric conductivity varies within wider limits than the main mechanical parameters, the pressure and mass velocity (the pressure in the detonation wave front exceeds the Chapman–Jouguet pressure typically by 30%). Therefore, electroconductivity measurements are potentially more sensitive and, in addition, yield information independent of the mechanical parameters. On the other hand, side reaction products, which produce only a minor effect on the energetics of the process, may prove important for electroconductivity measurements. The quasi-equilibrium mechanism of electric conduction, which is primarily determined by the thermodynamic conditions, can also contribute [4]. Note, however, that, in this case, the reaction zone (chemical spike) can also be discerned in the electroconductivity–time profile. Only experiments can elucidate how useful the electroconductivity method may prove in studying the reaction zone.

Most of the experiments performed to date have had insufficient resolution and provided only approximate information. In [3], due to the use of a differential cell, a satisfactory resolution was achieved but only at a fairly low electroconductivity, fractions of $\Omega^{-1}$ cm$^{-1}$, values typical of many loose-packed HEs. What role the initial density, an important characteristic of HEs, plays has remained unknown.

In the present work, we modified the differential method described in [3] so as to obtain a resolution high enough to perform measurements in dense HEs. The results for the most common HEs, detonating without the formation of large amounts of carbon, such as hexogen (RDX), octogen (HMX), and pentaerythritol tetranitrate (PETN) are presented. Some preliminary results were reported in the short communication [5].

## 2. A REVIEW OF THE EXPERIMENTAL METHODS

To study the structure of a detonation wave with a reaction zone narrower than 1 mm, the electroconductivity should be measured with a submillimeter resolution at least, a task that can be accomplished only with the help of electrocontact methods.

The most obvious interference is electric current spreading: when the electrodes are brought in contact with a conducting medium, the conductance is determined by a finite conducting region. The resolution width is typically on the order of the size of the cell's electrodes [6]. The use of thin electrodes is prohibitive because of the aggressive effect of the flow. It is known that metallic surfaces subjected to the action of detona-

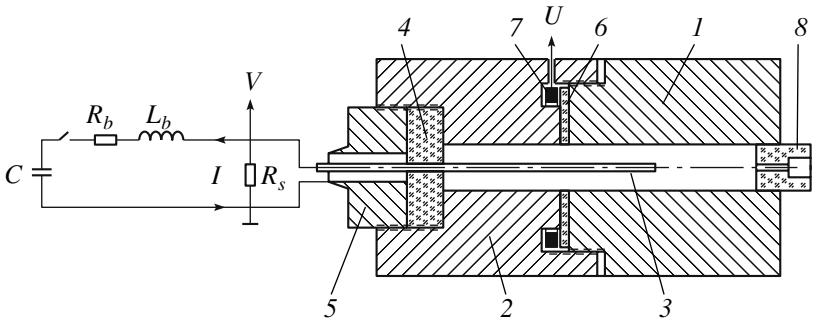


**Fig. 1.** Experimental setup.

tion products exhibit pits several tenths of a millimeter in size. Thus, a controllable geometry of measurements must be ensured by using electrodes not less than 1 mm in diameter. A detailed analysis of the effect of current spreading is examined in the appendix. Similar limitations arise due to the influence of gasdynamic factors, for example, the reflection of the detonation wave from the electrode.

Current spreading is operative in a uniformly conducting medium behind the wave front. A more subtle effect is associated with spatial nonuniformities of the electroconductivity σ. The distribution of the potential φ in a nonuniform medium is described by the equation [3]

$$\nabla^2\varphi + \frac{(\nabla\sigma\nabla\varphi)}{\sigma} = 0. \quad (1)$$

If the electric field has a component directed along the electroconductivity gradient, a spatial charge with a density of $(\nabla\sigma\nabla\varphi)/4\pi\sigma$ arises. Since the distortion of the field depends on the measured, initially unknown σ distribution, the resolution is determined by the characteristic size of electroconductivity variation.

Most of the measurement configurations used by different authors [1, 2, 4] are liable to all of the considered interferences. The simplest cells are suitable only for measuring slowly changing electroconductivity [6]. With a spatial resolution of tenths of a millimeter, the differential cell has tangible advantages [3]. In the current work, we used an upgraded cell of this type, described in the next section.

## 3. EXPERIMENTAL SETUP

We employed a coaxial arrangement of electrodes (Fig. 1). A charge with a diameter of $b = 8$ mm was pressed into a thick-wall copper confinement (*1*, *2*) 40 mm in diameter. Axial copper electrode *3* with a diameter of $c = 2$ mm was secured in Plexiglas stopper *4* fixed with hollow bolt *5*. A cavity in the external electrode accommodated electroconductivity sensor *7*, a toroidal coil. The coil–cavity contour mutual inductance *M* was 15 nH. Parts *1* and *2* of the external electrode were attached to each other via a screw joint. The thickness of the slit between parts *1* and *2* was preset by dielectric layer *6* (0.3 mm of Teflon or 0.3–1.0 mm of Plexiglas). When the detonation wave arrives at the coaxial electrode, the cell circuit becomes connected by the conducting region behind the detonation front. The electric current passing through the cell flows around the sensor cavity, thereby inducing a magnetic flux through the coil and, hence, a voltage pulse across its terminals. Later, when the detonation front travels past the slit, part of the current begins to flow via external electrode *2*. As a result, the strength of the current overflowing the cavity and, consequently, magnetic flux decrease, producing in the sensor a voltage pulse *U* of opposite polarity, with the electroconductivity in the plane of the slit being proportional to $U(t)$ [3]:

$$\sigma(x) = \frac{\ln(b/c)}{2\pi DM}\frac{U(t)}{V}. \quad (2)$$

Here, $x = Dt$ is the distance the front moved off from the slit by time *t* after passing it, *D* is the detonation velocity, *V* is the voltage across the electrodes produced by the feeding current *I* passing through resistor $R_s$ connected in parallel with the conducting region of the charge. The cell was fed by capacitor *C* (100 μF, 1000 V) connected to the circuit through a chain composed of resistor $R_b$ and induction coil $L_b$.

The actual voltage *U* differs somewhat from the experimentally measured one $U_{in}$ because of the effect of coil self-inductance ($L \approx 1$ μH), being related to it by the formula $U = U_{in} + (L/R)dU_{in}/dt$, where *R* is the input resistance of the oscilloscope (50 Ω). Since the calculation procedure involved differentiation, the signal was spline-smoothed to suppress small-scale noises.

The cell depicted in Fig. 1 renders electric current spreading unimportant, since the conductance of a strictly specified layer (between the detonation wave front and the plane of the slit) is measured. Since the electric field vector is perpendicular to the electroconductivity gradient nearly everywhere, the space charge effect is negligible (Eq. (1)). Another advantage of the cell is its ability to keep the intensity of gasdynamic perturbations as low as possible. A thin slit causes only a slight rarefaction, in contrast to shock waves typical of most experimental setups.

The resolution of the method is determined by the slit width $2a$. Analytical estimates and direct numerical calculations of the electric current distribution over the cell space (appendix) demonstrated that an optimal estimate of the experimental resolution is one-quarter of the slit width, $a/2 = 0.075$ mm ($2a = 0.3$ mm).

The differential scheme used in [3] included an external measuring contour, a short wire with an inductance of ~50 nH. The main advantage of the new, completely coaxial scheme is a fairly low inductance of the cavity contour $L_c$ (less than 1 nH). This makes it possible to substantially extent the range of measurements, up to $\cong 10\ \Omega^{-1}\ \text{cm}^{-1}$, instead of fractions of $\Omega^{-1}\ \text{cm}^{-1}$ [3]. The limitation is associated with an electric current flowing through a conducting medium above the slit under the action of the parasitic voltage $L_c dJ/dt$. Note that a similar low-inductance scheme was used in [7], but in a less convenient plane configuration.

Pressing was performed in 5-mm portions, so as to make the slit be located at the middle of a portion. At each HE density, we performed from two to four experiments. The uniformity of pressing grew increasingly perfect with the density. The charges were initiated by electric detonators through Plexiglas stopper *8* (Fig. 1) with a 2.4-mm axial channel filled with RDX. Thus, the main charge was initiated 40 mm from the plane of the slit and within 1.2 mm from the axis. This deviation might cause a scatter in the distance of travel of the wave to the slit less than 0.24 mm (if the detonation front is a segment of a sphere with the center at the point of initiation). In reality, the effect of the walls makes this scatter smaller—according to electroconductivity measurements, the scatter in pulse widths was less than 0.05 mm. Even less than 8-mm-in-diameter charges of the HEs under study detonate reproducibly without confinement, let alone detonation in a massive copper confinement. Control experiments with loose-packed HE charges confirmed the results reported in [3].

## 4. EXPERIMENTAL PROCEDURE AND DATA PROCESSING

Typical signals obtained in experiments with pressed PETN are displayed in Fig. 2. We used a digital oscilloscope with a bandwidth of 200 MHz and a sampling interval of 4 ns. The negative-polarity signal (upper trace) near the trigger point 0 μs was induced by the starting current generated by connection of the cell. This first peak, along with the voltage curve $V(t)$, was used to calibrate the sensor (determination of the coefficient $M$) immediately in the course of the experiment. In the simplest case, when the feeding current is constant, $R_s\int_0^t U dt = M(V_0 - V)$. In reality, during the experiment, the voltage at feeding capacitor $C$ is nearly constant, while the current varies somewhat. To limit the current growth rate upon switch-on of the feeding circuit, the external circuit inductance was selected to be relatively large (~15 μH), while the resistance value was moderate, $R_b \sim 17\ \Omega$, so as to enhance the current strength. As a result, the external circuit produces a marked effect on measurements, and, therefore, a more complex equation should be solved:

$$M(R_b + R_s)(V_0 - V) = R_b R_s \int_0^t U dt + L_b R_s U + M L_b (dV/dt).$$

We adjusted the $M$ so as to obtain the best fit between the calculated and measured $V(t)$ dependences. As a result, the calculated and measured curves visibly coincided with one another in the plot, with the error of determination of $M$ being within 1%.

The main signal from the coil, $U$, appears at 2.2 μs. Since its polarity is opposite to that of the first peak, the calibration curve begins to deviate from the $V(t)$ curve as soon as the wave travels past the slit (branch $V_c$ in Fig. 2). In an ideal case, the $V_c$ curve should return to the level $V_0$ (the surface areas of the first and second peaks $U$ are equal). Indeed, it nearly returns, a behavior indicative of the uncertainties associated with the possible mechanical deformation of the coil cavity being small. In some experiments, the return was not complete because of the slit being short-circuited, for example (see below). The moment when short-circuiting occurs is clearly seen, and, therefore, the signal before this moment can be considered truthful. Note that, in Fig. 2 starting from 3.9 μs, the switch-off of the current produces no signal from the electroconductivity sensor, an observation indicative of an effective uncoupling of the measurement contour and feeding circuit.

The characteristic points in the oscillograms and the known cell dimensions were used to determine the detonation velocity $D$. The measured velocities proved to be systematically lower than the ideal detonation velocity (i.e., the velocity of a steady detonation wave propagating in large-diameter charge) at the given expected charge density. For example, for the experimental results displayed in Fig. 2, the expected charge density was $\rho_e = 1.6\ \text{g/cm}^3$ while the measured detonation velocity was $D = 7.67$ km/s, a value that corresponds to a density of $\rho_D = 1.58\ \text{g/cm}^3$ for ideal detonation (1.2% lower than $\rho_e$) [8]. For PETN, we obtained a linear correlation $\rho_D = 0.982\rho_e$. The difference between $\rho_D$ and $\rho_e$ may be associated with the loss of some material during pressing, deformation of the confinement, and attenuation of the wave due to the expansion of the confinement. Weighing the experimental setup yielded values intermediate between $\rho_e$ and $\rho_D$. The accuracy of weighing of a relatively small charge in a heavy copper confinement prevented us from drawing more definite conclusions. In what follows, the initial density was identified with $\rho_D$, since the latter correlates with the experimentally measured detonation velocity; $\rho_D$ was calculated based on the data from [8]. This is the lower

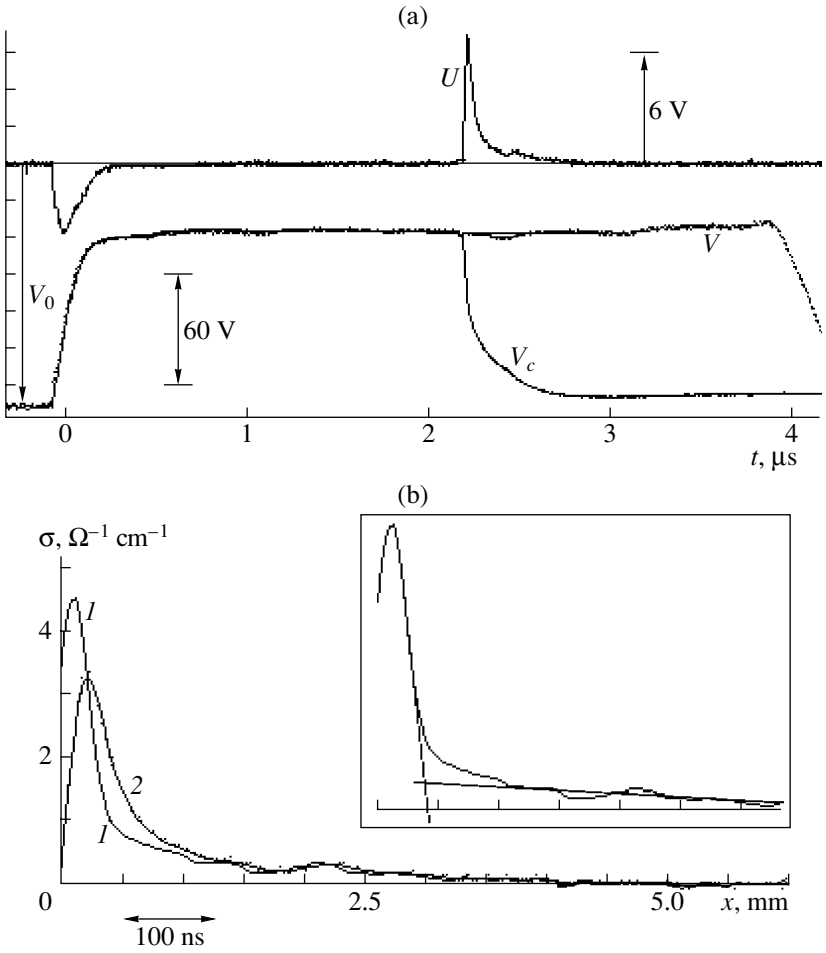


**Fig. 2.** (a) Recorded signals $U$ and $V$ for PETN with a density of 1.58 g/cm$^3$; $V_c$ is the calibration curve. (b) (*1*) Processed electroconductivity profile and (*2*) the original profile smoothed by the inductance of the sensor.

estimate of the density, without regard to detonation nonideality.

The electroconductivity–time profile calculated by formula (2) is shown in Fig. 2b (curve *1*). The slit width was 0.6 mm (Plexiglas layer), which corresponds to a theoretical resolution of 0.15 mm. The HEs studied are characterized by a nonuniform distribution. First, a peak with an amplitude of 4.5 $\Omega^{-1}$ cm$^{-1}$ appears, which is accompanied by a tail with a markedly lower ($\cong$0.5 $\Omega^{-1}$ cm$^{-1}$) and smoothly decaying electroconductivity. The experimental curve (*1*) is compared to curve *2*, which was obtained from the signal $U_{in}$ without corrections for the inductance of the coil. This curve is, in fact, a scaled oscillogram; it is smoother than curve *1* and merges with it in the tail region. In what follows, only corrected curves are demonstrated.

The initial jump in the electroconductivity signal was typically 70–80% of its amplitude. Since the maximum was attained just a little bit later, the delay in its attainment may be attributed to uncertainties in measurements and data processing—in reality, it may coincide with the front. The width of the peak was determined from the intersection of the tangent to the descending side of the peak with the linear approximation of the tail (inset in Fig. 2). In this case, the peak width was 0.39 mm.

In experiments with the central electrode shortened so as to escape electric current generation near the slit, no signal from the coil was recorded, which means that the polarization of the HE or the insulator produced no tangible effect.

## 5. EXPERIMENTAL RESULTS

In the experiments with PETN at $\rho$ = 1.72 g/cm$^3$ (Fig. 3), the charge weight was calculated based on a density of 1.8 g/cm$^3$, which is higher than the maximum theoretically possible one (1.77 g/cm$^3$), with the aim of approaching the latter. In this case, the charge was markedly more uniform (the signal $V(t)$ was smooth, in contrast to Fig. 2, in which small oscillations correlating with the boundaries of pressed portions were observed). As the initial density increases, so does the electroconductivity, while the peak width decreases.

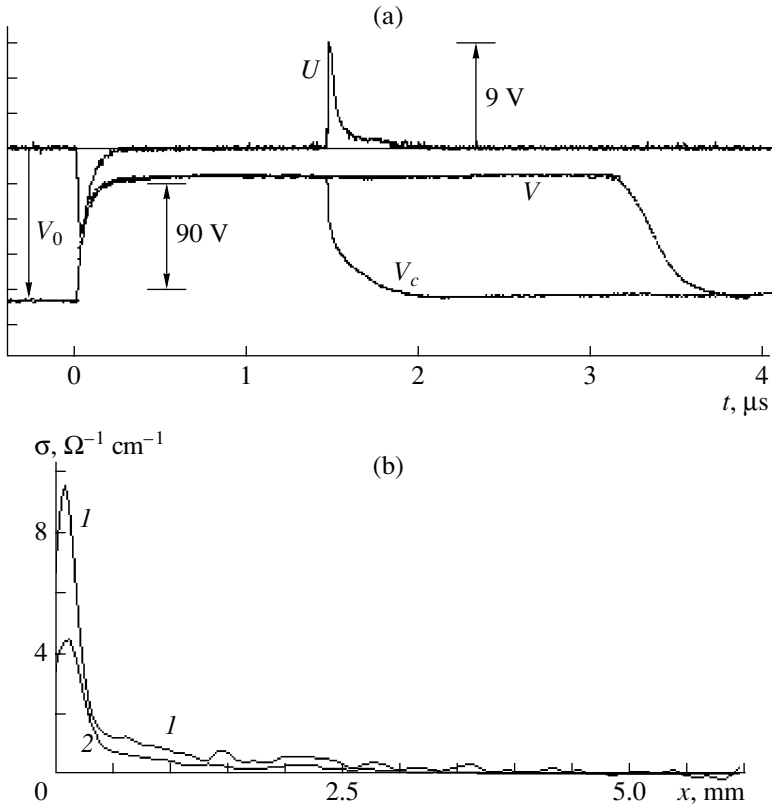


**Fig. 3.** (a) Recorded signals $U$ and $V$ for a PETN charge with a density of 1.72 g/cm$^3$. (b) The electroconductivity profiles for (*1*) this run and (*2*) the run performed at a PETN density of 1.58 g/cm$^3$.

Figure 3b shows the calculated electroconductivity–time profile (curve *1*). For comparison, the profile obtained at moderate density (curve *2*, identical to curve *1* in Fig. 2) is also presented. At PETN densities from 1.0 to 1.5 g/cm$^3$, we failed to obtain a uniform density of pressing. At a pour density (≈1 g/cm$^3$), the electroconductivity at the peak's maximum and peak width were ≈0.3 $\Omega^{-1}$ cm$^{-1}$ and 0.58 mm, respectively; the electroconductivity in the tail region was at least an order of magnitude lower than the maximum one.

The experiments with RDX and HMX also demonstrated that the maximum electroconductivity increases with the charge density. Note that the short-circuiting of the slit for the RDX charge occurs relatively rapidly, especially for a thin slit. Figure 4 shows the experimental results obtained at a density of 1.63 g/cm$^3$ at a slit width of 0.3 mm (filled with Plexiglas). The main signal $U$ decays to zero at instant of time of 2.2 μs, i.e., 0.3 μs after the beginning. In this case, the calibration curve does not return to the initial level, which means that the short-circuiting of the slit occurs in the tail region.

When a thicker insulator (0.6 mm) was used, short-circuiting occurs later. A comparison of the electroconductivity–time profiles recorded in these experiments (Fig. 4) demonstrated a close agreement between the times elapsed before short-circuiting. Curves *1* and *2* represent the experiment in which the slit widths were 0.3 and 0.6 mm, respectively. For the wider slit, the resolution is lower, but the measurement duration is longer. The peak widths were 0.38 and 0.37 mm, respectively. That the profiles *1* and *2* in Fig. 4 match well with each other shows that a 0.6-mm-wide slit fixed with a Plexiglas layer is an optimal choice; therefore, it is this configuration that was used in most of the experiments performed in the present work. The profile for a loose-packed RDX charge is also shown (curve *3*, $2a$ = 0.3 mm, Teflon insulator); as can be seen, it differs significantly from the profiles recorded for the pressed HE charges. For RDX, a linear correlation $\rho_D = 0.953\rho_e$ over a density range of 1.6–1.8 g/cm$^3$ was obtained.

Interpretation of measurements in HMX at the utmost densities proved to be more complex. Figure 5 shows the results obtained in two experiments with HMX charges of densities 1.7 g/cm$^3$ (a) and 1.8 g/cm$^3$ (b) (the correlation for HMX was found to be $\rho_D = 0.944\rho_e$. Even an approximate comparison of the integral signals $V$ is indicative of a significant difference in the behavior of the electroconductivity, with the electroconductivity for the denser charge being substantially higher (lower level of the voltage $V$). At the same time, the processing of the signals according to the standard procedure revealed no marked difference, even yielding a somewhat lower amplitude of the peak at the denser charge (cf. curves *1* and *2* in Fig. 5c).

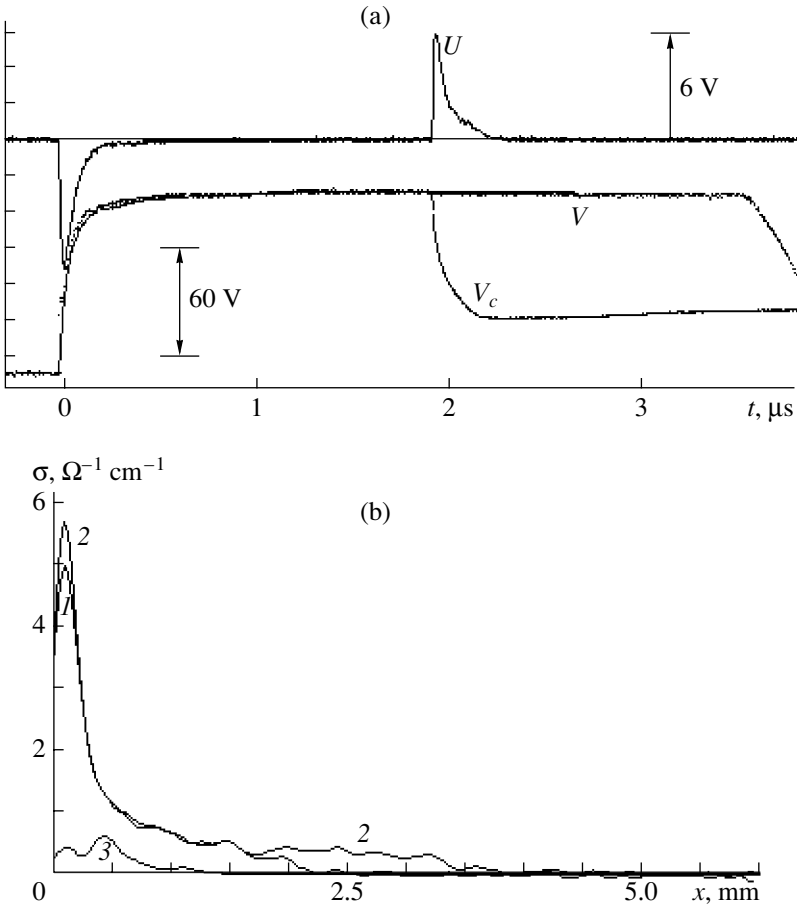


**Fig. 4.** (a) Recorded signals $U$ and $V$ for a RDX charge with a density of 1.63 g/cm$^3$ at a slit width of 0.3 mm. (b) (*1*) The electroconductivity profiles for this run, (*2*) a run at the same density but at a slit width of 0.6, and (*3*) at a pour density.

In our opinion, this discrepancy can be explained in part by a leakage current flowing through the conducting medium above the slit. When the electroconductivity near the slit is high, the switchover of the cell's current to electrode *2* may be delayed, causing a decrease in the $U$ signal. As can be seen from Fig. 5, the calibration curves fail to return to the initial level, especially in case *b*. In both cases, the short-circuiting through metal parts occurs at an instant of time of about 2.4 μs, with the $U$ signal exhibiting a well-pronounced "tail" before that moment. It is also seen that the steepest-descent segment of the $V_c$ curve, $\Delta V_c$, in Fig. 5b is markedly smaller than the analogous segment in Fig. 5a (the values of $\Delta V_c$ were calculated from the peak width, in both cases ~40 ns). This means that, at the higher density, part of the peak of the $U$ signal is lost. The data displayed in Fig. 5 suggest that the $V_c$ curves can be matched with each other by increasing the surface area encompassed by the $U(t)$ peak in Fig. 5b by a factor of ~1.5; i.e., the maximum electroconductivity should exceed 10 $\Omega^{-1}$ cm$^{-1}$.

In the electrotechnical approximation, the effect is determined by the leakage resistance $R_l$ and the self-inductance $L_c$ of the sensor cavity. For example, instead of a jumplike rise, the measured quantity $U(t)$ will grow within a time of $\approx L_c/R_l$. Under our experimental condition, the resistance of the medium above the slit was on the order of $1/(b\sigma)$. At $\sigma = 10\ \Omega^{-1}$ cm$^{-1}$ and $L_c = 0.9$ nH, $L_c/R_l \approx 7$ ns. For a 40-ns-wide peak, 18% of its surface area is lost because of the effect of leakage current. As the current in the cavity circuit steadies, the signal from the coil becomes adequate (profile *2* in Fig. 5 at $x \geq 0.25$ mm). Note, however, that the experimentally measured loss is substantially larger, $\Delta V_c$: ≈33% (Fig. 5). In addition, for PETN, no leakage was observed at the same level of electroconductivity (Fig. 3).

That a leakage current manifests itself in experiments with a dense HMX can be accounted for by the interaction of the detonation front with the insulator, for example, the mixing of insulator material with reacting HE, a process that may cause a local rise in the integral conductance of the cell upon arrival of the detonation wave at the endplate (Fig. 5), 3.525 and 3.4 μs for cases (a) and (b), respectively. At a high density, the voltage $V$ across the charge recovers markedly more slowly. Note also that, in all cases, the switch-off of the cell occurs substantially more slowly than one might expect by assuming that the electroconductivity at the bound-

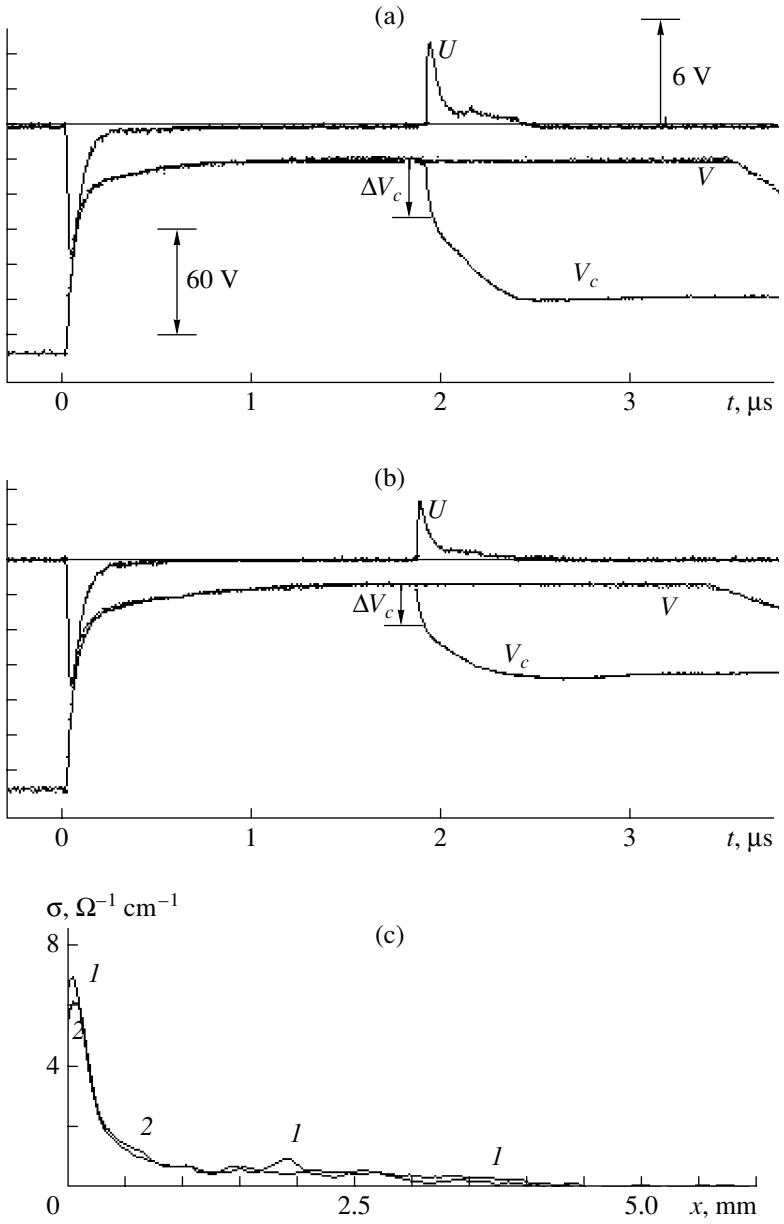


**Fig. 5.** (a) Recorded signals $U$ and $V$ for a HMX charges with densities of (a) 1.7 and (b) 1.8 g/cm$^3$. The slit width, 0.6 mm; the insulator, Plexiglas. (c) The electroconductivity profiles obtained.

ary disappears in accordance with the measured profile (compare the rates of recovery of $V$ and $V_c$ in Figs. 2–5).

The significant integral conductance at a high HMX density can also be explained by the peak becoming broader without growing in amplitude. Integral measurements [6] showed that such an effect exists indeed. Note, however, that integral experiments are of little value if the electroconductivity changes sharply (Section 2 and Appendix). In addition, as can be seen from Fig. 5, the oscillograms recorded in the differential-mode experiments exhibit no broadening, with the tail showing no significant growth with increasing density; i.e., the alternative explanation should also invoke the idea of enhanced leakage. Anyway, for highest density HMX, this method appreciably distorts the results, and the maximum value of ~10 $\Omega^{-1}$ cm$^{-1}$ must be considered only an estimate. Recall that the value of $\sigma$ = 10 $\Omega^{-1}$ cm$^{-1}$ for HMX with a density of 1.8 g/cm$^3$ was obtained by V.V. Yakushev [9].

The highest values of the electroconductivity at the peak's maximum for the three HEs under study are presented in Fig. 6. Each point was obtained by averaging several values; the measurement error was estimated to be 20%. For highest density HMX, a range of values is indicated, with the upper boundary being an estimate. The widths of the electroconductivity peaks as func-

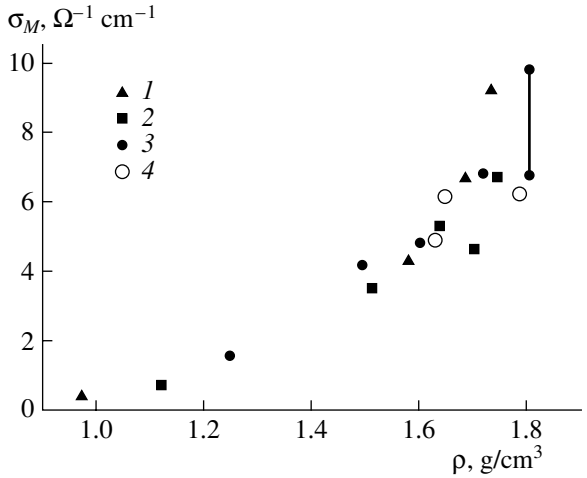


**Fig. 6.** Dependence of the electroconductivity at the peak maximum on the HE density: (*1*) PETN, (*2*) RDX, (*3*) HMX, and (*4*) fine-grained HMX.

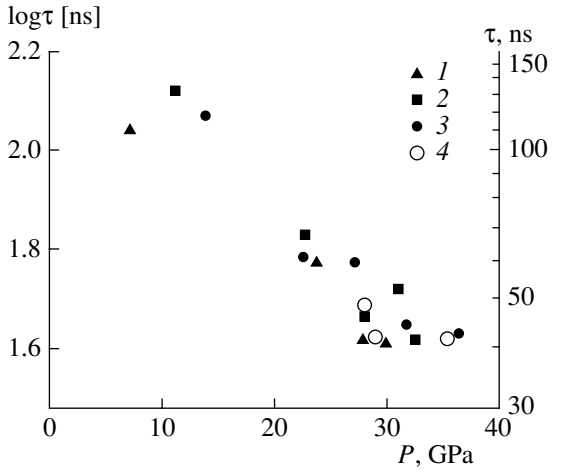


**Fig. 7.** Dependence of the electroconductivity peak width on the Chapman–Jouguet pressure. For notations, see Fig. 6.

tions of the Chapman–Jouguet pressure are displayed in Fig. 7. This dependence is similar to that used in [21]. The pressure was calculated by the formula $P = \rho D^2/(k + 1)$ using the $k$ values borrowed from [8].

## 6. DISCUSSION OF THE EXPERIMENTAL RESULTS

RDX and HMX have the same elemental composition, and their electroconductivities at the maximum of the peak at a given density of the charge differ only slightly. This is indicative of the similarity of the medium in the electroconductivity peak region and, probably, of the similarity of the chemical reaction involved. The electroconductivities at the maximum of the peak recorded in experiments with PETN charges, except, perhaps, highest-density ones, are close to those observed for RDX and HMX (Fig. 6). The widths of the peaks, however, differ somewhat, being the shortest in PETN (Fig. 7). The results obtained for fine-grained HMX (5 μm) were essentially identical to those obtained for coarse-grained HMX (200–300 μm) (Figs. 6 and 7).

The structure of detonation waves has been studied in many works, starting from [10]. The results of an extensive set of measurements with the use of the electromagnetic method were reported in [11]. Later [12, 13], the resolution of the method was improved and fast-response optical techniques appeared, in particular, for measuring the velocity of the HE–window material interface [14–19]. The emission from the shock front at the moment of its passing from the HE into the indicator liquid [20, 21] and the velocity of the wave that passed [22] were measured. The results of these measurements are often contradictory. Electromagnetic measurements yielded a reaction zone width of ~1 mm (~100 ns) [11], while optical data are indicative of a substantially smaller value, ~0.3 mm (~40 ns). These discrepancies can be explained in part by the use of different definitions of the reaction zone [21].

In our experiments, we obtained widths of the electroconductivity peaks in pressed HEs of 40–70 ns (Fig. 7). Generally, our results compare favorably with reaction zone widths measured by various optical methods. Note that the number of data suitable for comparison is limited. The focus of most current studies is on various high-density compositions containing a binder. The detonation of pure PETN, RDX, and HMX, the reactions in which are not complicated by the presence of admixtures, were studied in [14–21]; agatized (pressed with acetone to a density of 99% of the maximum one) HEs, in [15, 16, 21, 22]. Only the authors of [18, 19] performed experiments by varying the initial density within a wide range; when reported, the widths of the peaks of the interface velocity were close to our results (30–70 ns). The data from [20, 21] are also in satisfactory agreement with our measurements, except for agatized HEs. In the experiments performed in [15–17] with pure HEs, the chemical spike was masked by flow pulsations, the main object of these studies; therefore, a meaningful comparison was difficult to conduct. The earlier results presented in [11] differ from ours (the reaction zone is two to three times wider), which is unsurprising, given the low resolution of electromagnetic measurements in [11] (~100 ns). Qualitatively, the effect of the initial density reported in [11] was similar (in fact, somewhat stronger) to that observed in our experiments. Therefore, we believe that, for the HEs under study, in the density range covered, the reaction zone width is close to the width of the enhanced electroconductivity region.

At the highest densities (99% of that of the crystal), many studies detected an acceleration of the reaction. The authors of [22] revealed that agatized HEs exhibit no chemical spike, a result confirmed later in [21]. This

was interpreted as a rather sharp narrowing of the reaction zone, below the resolution of the available methods (~5 ns). In [18, 19], it was found that, in detonating RDX and HMX charges containing 1% acetone, the chemical spike disappeared at densities of above 1.72 g/cm$^3$ and 1.84 g/cm$^3$, respectively; instead of decreasing, the pressure behind the front rose. In contrast to [21, 22], for charges pressed to the maximum density with a standard amount of acetone (10%), the authors of [18, 19] observed a ~30-ns chemical spike, as did the authors of the study [16], in which, however, the spike width was not indicated, being, probably, substantially smaller. Analyzing the data for PETN with a porosity of 1% obtained at a resolution of 4 ns [14], the authors failed to reveal any chemical spike.

In our experiments, the chemical spike width decreased smoothly with increasing density, without noticeable irregularities, even at the highest densities. In principle, the initiation configuration used in the current work permits a skewing of the detonation wave front large enough to broaden the peak by up to 30 ns. Note, however, that the scatter in the measured values was much smaller, with a standard deviation of ~5 ns; the shortest width was 36 ns (for RDX with a density of 1.74 g/cm$^3$). The absence of marked irregularities may be associated with the charge structure being different. It also cannot be excluded that the densities attained fall short of that needed (the maximum densities for PETN, RDX, and HMX were 1.73, 1.74, and 1.8, respectively, as estimated from the detonation velocity). In the preliminary report [5], the dependence of the peak width on the density of RDX turned out to be sharper, probably because of a skewing of the front upon initiation. By the way, the results of optical measurements at the highest densities are also contradictory, a situation calling for further work.

At present, only a preliminary theoretical analysis of electroconductivity data is achievable. As can be easily seen, under typical conditions behind the front of a detonation wave (with a density of ~2 g/cm$^3$ and a temperature of several thousand kelvins), all the characteristic lengths (intermolecular distance, free path, reciprocal electron wavevector, and molecular size) are on the order of $3 \cdot 10^{-8}$ cm. Such a medium can be thought of as an intermediate state hardly accessible for studies by means of traditional method applicable to condensed-state and plasma physics. For example, calculation of the ionization potential drop by the formula used in plasma physics, $\Delta I \cong e^2(4\pi n/3\zeta)^{1/3}$ [23], at a packing factor of $\zeta = 0.64$ yields 10 eV. Such a high value, comparable with the ionization potentials of a number of detonation product molecules, cannot be considered a correct and, hence, a reliable value.

According to [4, 24], the electroconductivity of the detonation products may be associated with the formation of ions of water, a compound comprising a substantial fraction of the detonation products. Indeed, aqueous solutions of salts contain ions even at room temperature. Water also dissociates, especially at elevated pressures and temperatures. Water dissociation is expected to ensure an electroconductivity of 1 to 4 $\Omega^{-1}$ cm$^{-1}$. One advantage of this estimate is that it is based on numerous experimental data on the electroconductivity of shock-compressed water, which are indicative of a significant degree of dissociation at pressures near 200 kbar [25–27]. Recent experiments [28] confirmed that the electroconductivity of water at pressures below 1 Mbar (100 GPa) is of ionic character but becomes electronic at pressures appreciably above 1 Mbar. Unlike water, a relatively simple medium, the substance in the reaction zone of the detonation wave is a challenging object to study.

We believe that, in the HEs studied, the ionic conductivity is predominant in the tail, which begins exactly at an electroconductivity of $\cong 1$ $\Omega^{-1}$ cm$^{-1}$ and becomes more pronounced at high density, a behavior indicative of the degree of ionization increasing with the temperature and pressure. At a pour density, we observed no tail. Note that, at a slower decrease in the parameters, characteristic of large-diameter charges, the tail was observed even at the pour density [4, 29]. The maximum recorded electroconductivity (up to 10 $\Omega^{-1}$ cm$^{-1}$) is difficult to account for within the framework of the ionic mechanism. Near 300 kbar, the electroconductivity of water is only weakly dependent on the pressure, and, therefore, a moderate increase in the pressure in the reaction zone cannot explain why the peak arises, nor can the highly unrealistic idea of existence of large superequilibrium concentrations of water. The dissociation of intermediate reaction products is also unlikely to resolve the problem, since water, producing $H^+$, the most mobile ions, is viewed as the most promising candidate.

On the other hand, the nonequilibrium reaction zone comprises a wide variety of fragments of the initial molecule, including readily ionizable ones. Since electrons are substantially more mobile than ions, they can give rise to conduction at relatively low concentrations. In addition, intermediate products can participate in associative ionization reactions with one another. For example, the nonequilibrium ionization of flames is commonly attributed to the reaction [30]

$$CH + O \longrightarrow CHO^+ + e^-.$$

In this case, the energy spent to produce an electron is lower than the ionization potential of CHO by the dissociation energy of the bond formed. In particular, the endothermicity of this reaction under flame conditions is 0.35 eV [31]. It stands to reason that, at high densities, reactions of this type may become exothermic.

An intriguing possibility is the existence of a superequilibrium concentration of carbon in the reaction zone [32]. Carbon particles can produce a conductance pulse by forming conducting chains [2] or via thermionic emission [33]. The growth of the carbon yield at high densities may manifest itself in the tail region.

## 7. CONCLUSIONS

An electroconductivity method for studying the structure of detonation waves in dense HEs was developed. The measuring cell performs instrumental differentiation of the conductance of a well-defined region of the medium. The range of measurements was substantially extended, up to 10 $\Omega^{-1}$ cm$^{-1}$.

The distribution of electroconductivity behind the front is highly nonuniform. The conductance pulse is produced by chemical reaction, and, therefore, it has a nonequilibrium character. The pulse is accompanied by a tail, with largely equilibrium conductance (determined by the thermodynamic conditions). As the density increases, so does the peak maximum electroconductivity, while the peak width decreases. The peak widths for PETN, RDX, and HMX correlate with the available optical data on the reaction zone size. At the highest densities, no appreciable decrease in the pulse amplitude was observed.

## 8. APPENDIX: MODELING OF CURRENT SPREAD

**Integral cell.** We considered a two-electrode coaxial cell with an external diameter of $b = 8$ mm and an internal diameter of $c = 2$ mm. We numerically solved Eq. (1) for the potential $\varphi(r, z)$ with the following boundary conditions: $\varphi = 0$ at the external electrode, $\varphi = 1$ at the internal electrode, and $\partial\varphi/\partial z = 0$ at the detonation front ($z = 0$) and at a large distance ($z = 4$ mm) from the front. We used an iteration method with centered difference scheme; the step along both coordinates was $h = 0.02$ mm.

At various depths of immersion of the central electrode into the conducting medium, the integral conductance of the cell $Y$ was calculated from the potential distribution, after which an analytical expression for $Y(x)$ was constructed. When current spread is disregarded, $\sigma \propto dY/dx$. The error introduced by this formula is illustrated in Figs. 8a and 8b for a variable electroconductivity in the form of a step smoothed by a sinusoid half-wave with a drop from 7 to 1 $\Omega^{-1}$ cm$^{-1}$. The width of the peak was on the order of the spread width. The insets show a qualitative distribution of current lines. In Fig. 8a, the end face of the central electrode is flat. Curve *1* represents the calculated $Y(x)$ dependence. The jump that arises when the conducting medium arrives at the electrode is seen. Curve *2* is an approximation of $Y(x)$ by the superposition of two decaying exponents and a fourth-order polynomial. It deviates from the modeled dependence only within an initial segment ($x < 0.25$ mm), since it must pass through the origin of coordinates in order to make the derived electroconductivity finite. Curve *3* represents the apparent electroconductivity, it is obtained from dependence *2* by differentiation. It differs significantly from the true one (curve *4*), especially at small $x$ values. The error may be still higher (when the segment of deviation of curves *1* and *2* is shortened), in theory unlimited. When the tip of the central electrode has a semispherical shape (Fig. 8b), a steep rise, $Y \propto \sqrt{x}$, appears instead of the initial jump, since the surface area of contact between the electrode and the conducting medium increases gradually. Approximation curve *2*, plotted with consideration given to this aspect (a third-order polynomial plus a term proportional to $\sqrt{x}$) virtually coincides with calculated dependence *1*. In this version, curves *3* and *4* also differ from each other considerably.

When the longitudinal spreading is disregarded, the error becomes very large, with its scale being determined by seemingly unimportant details of data processing. At small $x$, the electroconductivity is overestimated, being underestimated at large $x$; the surface areas encompassed by curves *3* and *4* coincide. For a flat end surface at $x \approx 1$ mm, the derived electroconductivity is close to zero, a result that can be explained by a weakening of current spreading in a poorly conducting medium. Recently, such peculiarities, along with peak-maximum electroconductivity values nearly four times those measured in [3, 29], were observed in experiments with pour density HEs [34]. According to the modeling results obtained, precisely such peculiarities should be produced by the effect of spreading. Erroneous interpretations of experimental results have appeared due to a fundamental misunderstanding of the nature of the limitations imposed by current spreading on the resolution: instead of partial integration with signal smoothing, a frequently encountered situation, this mode of measurements involves partial differentiation.

We compared electroconductivity profiles obtained by the regular procedure described in Sections 3 and 4 and profiles that can be derived from the first peak in the $U(t)$ signal and the accompanying signal near $t = 0$. The modeling results were confirmed: profiles with a significant overestimation of the peak maximum electroconductivity, often with the subsequent decay to zero (or even negative values), were obtained. At the same time, a large scattering in these values was observed, which can be naturally attributed to a nonuniformity in the charge density near the tip of the electrode.

**Differential cell.** For the three-electrode cell (Fig. 1), the nonuniformity of the field is concentrated near the thin slit. Therefore, this configuration can be rather accurately treated within the framework of a planar problem. Electrodes *1* and *2* rotated so as to bring them into the horizontal plane were kept at zero potential, while the insulator and wave front had zero normal derivatives. Far from the slit, a vertical electric field of strength $E_0$ was set.

For a uniformly conducting medium, there exists an analytical solution to the problem, a feature that made it possible to test the calculation code. Let $\Phi(z) = \varphi + i\psi$ be a complex potential inside the first quadrant of a $z = x + iy$ plane such that the wave front coincides with

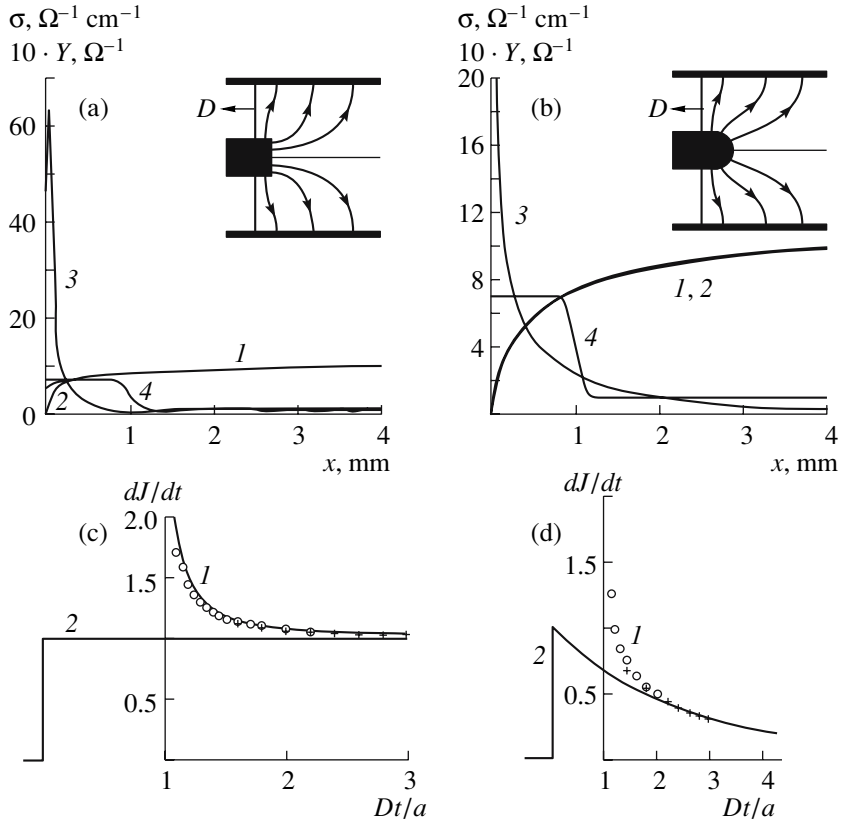


**Fig. 8.** Modeling results for (a, b) two-electrode and (c, d) three-electrode differential cell.

the $x = 0$ boundary while the slit occupies a segment within $Dt - a < x < Dt + a$ at the $y = 0$ boundary, with the rest of this boundary being a zero equipotential. It is easy to see that

$$\Phi = -iE_0(L + a)\left(E(\zeta, m) - \left(1 - \frac{E'}{K'}\right)E(\zeta, m)\right).$$

Here, $L = Dt$ is the distance from the wave front to the midpoint of the slit; $\zeta = z/(L - a)$; $F(\zeta, m)$ and $E(\zeta, m)$ are incomplete elliptic integrals of the first and second kind, respectively; $m = (L - a)/(L + a)$ is the modulus; $K'$ and $E'$ are complementary complete elliptic integrals of the first and second kind. At constant $\sigma$, the current per unit width of electrode 2 is $J = \pi\sigma E_0(L + a)/2K'$. The measured signal is given by $U(t) \propto dJ/dt$. Figure 8c shows the $dJ/dt$ profile against the background of an ideal signal (unit jump for an infinitely thin slit). Curve *1* is the analytical dependence, while the points represent the results of numerical calculations (circles and crosses correspond to calculation grids with 40 and 10 meshes per width $a$, respectively). As can be seen, the analytical and numerical results are in close agreement. We also performed calculations for the case where the insulator was indented into the silt a distance $a$ deep, but revealed no appreciable differences from the main variant. An accuracy of ≅20% is achieved after the wave has traveled a distance shorter than $0.5a$ along electrode 2. This value should be considered as a reasonable estimate of the resolution. As the front moves away from the slit, the error decreases as $(a/2Dt)^2$.

To estimate the effect of a weak nonuniformity in $\sigma$, we presented the potential as $\varphi = \varphi_1 + \varphi_2$, where $\varphi_1$ is the solution to the Laplace equation for a uniformly conducting medium (see above) and $\varphi_2$ is the correlation associated with the nonuniformity. For a given $\sigma(x)$ dependence, a space charge of density $\rho = -(E_{1x}/4\pi\sigma)(d\sigma/dx)$ arises. Since the field $E_{1x} = -\partial\varphi_1/\partial x$ is concentrated near the insulator, the value of $d\sigma/dx$ can be considered constant and equal to that in the slit. The vertical electric field at the electrode surface at a coordinate $s$ associated with the space charge in the vicinity of a point $(x, y)$ can be written as a component of the field of a charged filament:

$$dE_{2y} = 2\frac{2\rho y}{(s - x)^2 + y^2}dxdy,$$

with the factor 2 taking into account the image charges behind the horizontal plane. The correction to the current reads as

$$\Delta J = -\int_0^{L-a} \sigma E_{2y} ds$$

$$= -\frac{1}{\pi}\frac{d\sigma}{dx}\int_0^{L-a} ds \int_{x,y>0} \frac{yE_{1x}}{(s-x)^2+y^2} dxdy.$$

Using the asymptotic expression for $E_{1x}$ at $L \gg a$ and performing a number of cumbersome rearrangements, we obtained the following expression for the derivative of the current with respect to the time:

$$\frac{d\Delta J}{dt} = -\frac{E_0 a^2}{4\sqrt{2}} D \frac{d^2\sigma}{dx^2} \ln\left(\frac{\Delta}{a}\right),$$

where $\Delta = \sigma/(d\sigma/dx)$ is the characteristic size of change of in electroconductivity. Comparing this derivative with the derivative of the main current $\sigma E_0 D$, we found that the error associated with the nonuniformity of $\sigma$ is about $(a/2\Delta)^2 \ln(\Delta/a)$, i.e., of nearly second order in $a$.

Figure 8d shows the calculated response of the cell when the electroconductivity decays exponentially (at $\Delta = 2.5a$). Calculations confirmed that, under these conditions (corresponding to the characteristics of the experimental setup, $a = 0.16$ mm and $\Delta = 0.4$ mm), the nonuniformity of the medium produces only a slight effect on measurement results: as discussed above, the error associated with a space charge is below 4%.

## ACKNOWLEDGMENTS

This work was supported by the Russian Foundation for Basic Research (project no. 05-03-32412a) and INTAS (project no. 03-51-3332).

## REFERENCES

1. A. A. Brish, M. S. Tarasov, and V. A. Tsukerman, Zh. Eksp. Teor. Fiz. **37** (6(12)), 1543 (1959).
2. B. Hayes, in *Proc. 4th Symp. (Int.) on Detonation* (White Oak, MD, 1965), p. 595.
3. A. P. Ershov, P. I. Zubkov, and L. A. Luk'yanchikov, Fiz. Goreniya Vzryva **10** (6), 864 (1974).
4. A. G. Antipenko, A. N. Dremin, and V. V. Yakushev, Dokl. Akad. Nauk SSSR **225** (5), 1086 (1975).
5. A. P. Ershov, N. P. Satonkina, and G. M. Ivanov, Pis'ma Zh. Tekh. Fiz. **30** (4), 63 (2004) [Tech. Phys. Lett. **30** (4), 1048 (2004)].
6. A. P. Ershov, N. P. Satonkina, O. A. Dibirov, et al., Fiz. Goreniya Vzryva **36** (5), 97 (2000).
7. D. G. Tasker and R. J. Lee, in *Proc. 9th Symp. (Int.) on Detonation* (Portland, OR, 1989), p. 369.
8. L. V. Al'tshuler, G. S. Doronin, and V. S. Zhuchenko, Fiz. Goreniya Vzryva **25** (2), 84 (1989).
9. V. V. Yakushev, *Report at Int. AIRAPT Conf. on High Pressure Science and Technology* (Honolulu, Hawaii, USA, 1999).
10. R. E. Duff and E. Houston, J. Chem. Phys. **23** (7), 1268 (1955).
11. A. N. Dremin, S. D. Savrov, V. S. Trofimov, and K. K. Shvedov, *Detonation Waves in Condensed Media* (Nauka, Moscow, 1970) [in Russian].
12. B. Hayes, Rev. Sci. Instrum. **52** (4), 594 (1981).
13. P. A. Urt'ev, Khim. Fiz. **12** (5), 579 (1993).
14. C. M. Tarver, R. D. Breithaupt, and J. W. Kury, J. Appl. Phys. **81** (11), 7193 (1997).
15. A. V. Fedorov, Khim. Fiz. **21** (8), 66 (2002).
16. A. V. Fedorov, in *Proc. 12th Symp.(Int.) on Detonation* (San Diego, CA, 2005), p. 230.
17. A. V. Fedorov, Khim. Fiz. **24** (10), 13 (2005).
18. A. V. Utkin, S. A. Kolesnikov, and S. V. Pershin, Fiz. Goreniya Vzryva **38** (5), 111 (2002).
19. A. V. Utkin, S. A. Kolesnikov, S. V. Pershin, et al., in *Proc. 12th Symp. (Int.) on Detonation* (San Diego, CA, 2005), p. 175.
20. S. N. Lubyatinsky and B. G. Loboiko, in *Proc. 11th Symp. (Int.) on Detonation* (Village, CO, 1998), p. 836.
21. B. G. Loboiko and S. N. Lyubyatinskii, Fiz. Goreniya Vzryva **36** (6), 45 (2000).
22. V. K. Ashaev, G. S. Doronin, and A. D. Levin, Fiz. Goreniya Vzryva **24** (1), 95 (1988).
23. A. A. Likalter, Zh. Eksp. Teor. Fiz. **113** (3), 1094 (1998).
24. V. V. Yakushev and A. N. Dremin, Dokl. Akad. Nauk SSSR **221** (5), 1143 (1975).
25. S. D. Hamann and M. Linton, Trans. Faraday Soc. **62**, 2234 (1966).
26. A. C. Mitchell and W. J. Nellis, J. Chem. Phys. **76** (12), 6273 (1982).
27. V. V. Yakushev, V. I. Postnov, V. E. Fortov, and T. I. Yakusheva, Zh. Eksp. Teor. Fiz. **117** (4), 710 (2000) [J. Exp. Theor. Phys. **90** (4), 617 (2000)].
28. P. M. Celliers, G. W. Collins, D. G. Hicks, et al., Phys. Plasmas **11** (8), L41 (2004).
29. A. P. Ershov, P. I. Zubkov, and L. A. Luk'yanchikov, in *Detonatsiya* (Otd. Inst. Khim. Fiz. Akad. Nauk SSSR, Chernogolovka, 1977), p. 89 [in Russian].
30. H. F. Calcote, in *Progress in Astronautics and Aeronautics* (Academic, London, 1963), Vol. 12, p. 107.
31. H. Pritchard and A. G. Harrison, J. Chem. Phys. **48** (6), 2827 (1968).
32. V. F. Anisichkin, Fiz. Goreniya Vzryva **30** (5), 100 (1994).
33. A. P. Ershov, Fiz. Goreniya Vzryva **11** (6), 938 (1975).
34. P. I. Zubkov, P. I. Ivanov, A. M. Kartashov, et al., in *Proc. V Khariton Scientific Readings* (Ross. Fiz. Yad. Tsentr-Vserossiiskii Nauch.-Issledovate'skii Inst. Eksperimental'noi Fiziki, Sarov, 2003) [in Russian].